

Disorder, Pseudospins, and Backscattering in Carbon Nanotubes

Paul L. McEuen, Marc Bockrath, David H. Cobden,* Young-Gui Yoon, and Steven G. Louie

Department of Physics, University of California, and Materials Science Division, Lawrence Berkeley National Laboratory, Berkeley, California 94720

(Received 7 June 1999)

We address the effects of disorder on the conducting properties of metal and semiconducting carbon nanotubes. Experimentally, the mean free path is found to be much larger in metallic tubes than in doped semiconducting tubes. We show that this result can be understood theoretically if the disorder potential is long ranged. The effects of a pseudospin index that describes the internal sublattice structure of the states lead to a suppression of scattering in metallic tubes, but not in semiconducting tubes. This conclusion is supported by tight-binding calculations.

PACS numbers: 73.50.-h, 73.23.Hk, 73.61.Wp

Single-wall carbon nanotubes (SWNTs) are two-dimensional (2D) graphene sheets rolled into nanometer-diameter cylinders [1,2] that can either be 1D metals or semiconductors, depending on how the sheet is rolled up. This surprising behavior follows from the unusual band structure of a graphene sheet. It is a semimetal with a vanishing gap at the corners of the first Brillouin zone (BZ) where the π (bonding) and π^* (antibonding) bands touch at two inequivalent wave vectors \mathbf{K} and \mathbf{K}' [Fig. 1(a)]. As the Fermi level moves due to chemical or electrostatic doping, the Fermi surface becomes circular arcs at the corners of the BZ, as is shown in Fig. 1(a) for hole doping. This Fermi surface can be more simply represented in the extended zone scheme by piecing together the arcs to form Fermi circles of radius k centered around the \mathbf{K} (\mathbf{K}') point. When a graphene sheet is rolled up into a tube, the allowed wave vector components perpendicular to the tube axis become quantized, resulting in 1D subbands with allowed k 's represented by dashed lines in Figs. 1(b) and 1(c). For metallic tubes [Fig. 1(b)], one set of allowed wave vectors goes through the \mathbf{K} point and there are propagating modes at E_f at $+k$ and $-k$. This 1D mode has a linear (massless) dispersion, as is indicated in the figure. For semiconducting tubes [Fig. 1(c)], the allowed wave vectors do not go through the \mathbf{K} point. For small \mathbf{k} , there are thus no allowed states at E_f , but if the tube is doped sufficiently, the Fermi circle reaches the nearest 1D subband and propagating modes exist, whose (massive) dispersion is shown in the figure.

A wealth of scanned probe and electrical transport measurements have been performed to probe the electronic structure and conducting properties of SWNTs [2]. Overall, the experimental results agree with the predictions of band structure given above. Many interesting open issues remain, however, particularly concerning the effect of Coulomb interactions [3–6] and disorder [7–9] on the electronic states. For example, recent theoretical work has emphasized that the effects of disorder may be significantly reduced in metallic SWNTs for a number of reasons [7–9]. Experiments indeed give compelling evi-

dence that a *metallic* tube can have a very long mean free path ℓ on the order of a micron [10–14]. Initial experiments on doped *semiconducting* tubes, however, have yielded ℓ 's that are orders of magnitude shorter [15,16]. This is perhaps surprising, since the tubes are nearly structurally identical and the amount of disorder likely very similar. In this Letter, we address this apparent discrepancy between the properties of metallic and doped semiconducting nanotubes.

We begin by discussing the experimental evidence that ℓ can be very long in metallic SWNTs. Figure 2 shows a measurement of a nanotube rope $\sim 8 \mu\text{m}$ in length. At low T , Coulomb oscillations in the conductance G vs gate voltage V_g are observed as electrons are added to the rope [10,11]. Using the charging energy $U \sim 0.5 \text{ meV}$ determined from the T dependence, the effective length L_{eff} of the segment of tube to which the electrons are added can be estimated [10,11]. For this device, we find $L_{\text{eff}} \sim 10 \mu\text{m}$, which is approximately the physical tube

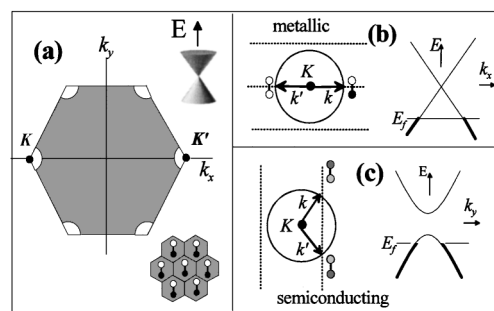


FIG. 1. (a) Filled states (shaded) in the first Brillouin zone of a single p -type graphene sheet. The sheet contains two carbon atoms per unit cell (lower right inset). The dispersions of the states in the vicinity of E_f are cones (upper right inset) whose vertices are located at the \mathbf{K} and \mathbf{K}' points. The Fermi circle around the \mathbf{K} point, the allowed k vectors, and their dispersion are shown in (b) and (c) for a metallic and semiconducting tube, respectively. The dumbbells represent the molecular orbitals comprising the states, with white-white, white-black, and gray dumbbells representing bonding, antibonding, and mixed orbitals, respectively.

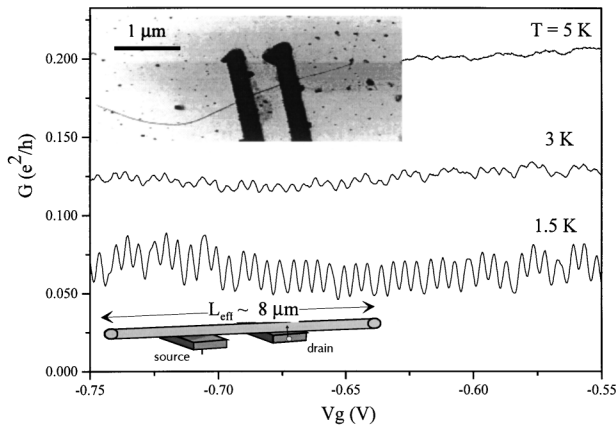


FIG. 2. Conductance versus gate voltage at different temperatures for the metallic nanotube device shown in the upper inset. All devices were prepared from unpurified nanotubes in the manner described in Refs. [6] and [11]. The 3 nm diameter and 8 μm long nanotube rope is draped over two contacts that make tunnel contact to a metallic tube in the rope. A voltage applied to the doped substrate is used to adjust the carrier density. The appearance of the CB oscillations only at very low temperatures (~ 1.5 K) indicates that the electrons are delocalized over the entire length of the tube, as indicated in the lower inset. The observation of a single, regular period in the Coulomb oscillations is strong evidence that a single metallic tube in the rope is determining the conducting properties [6,11].

length, as previously observed by the DELFT group [10]. Note that any significant backscattering within the tube would localize the electronic states on the scale of ℓ and effectively break the tube into a series of dots [17]. This would result in multiple Coulomb blockade periods as a function of V_g with larger charging energies. The observation of a single, well-defined, and small charging energy is thus very strong evidence that ℓ is many μm s in length.

Additional evidence for large ℓ 's comes from measurements of the two terminal conductance of nanotubes with near-Ohmic contacts. For perfect contacts, the conductance is predicted to be $G = (e^2/h)\Sigma T_i$, where T_i is the transmission coefficient for each of the four 1D channels propagating through the tube. Measurements by a number of groups [11,13,14] have yielded conductances $\sim e^2/h$, indicating that the T_i 's can be on the order of unity, even for tubes many microns in length. Clearly, then, metallic tubes can have mean free paths at the micron length scale.

We now turn to experiments on semiconducting tubes. Tans *et al.* [15] and Martel *et al.* [16] measured electrostatically doped p -type tubes and Bockrath *et al.* [18] measured n -type tubes that were chemically doped. These results can be analyzed using a model of a diffusive conductor. In the simplest version, transport through the tube is limited by scatterers spaced at a distance ℓ , each with transmission probability $T_i \sim \frac{1}{2}$. The conductance of a tube of length L is then $G \cong (4e^2/h)(\ell/L)$. Using the physical length of the tube and the maximum measured

conductance, these experiments indicate $\ell \sim 2$ nm at the largest carrier densities. This is 3 orders of magnitude shorter than the ℓ found above for metallic tubes.

To investigate this striking discrepancy further, we have performed extensive measurements on semiconducting tubes at both room and low temperatures. Figure 3 shows the G vs V_g measured for one device. At room temperature, the conductance increases as V_g is decreased and holes are added to the valence band of the semiconducting tube. (The saturation of G at large negative V_g is believed to be due to the contact resistance for tunneling into the tubes [15,16].) As T is lowered, G is suppressed and breaks up into a series of peaks as a function of V_g . At low temperatures ($T < 20$ K), G is immeasurably small at all V_g . The lower inset to Fig. 3 shows the differential conductance, dI/dV , for a different semiconducting tube device as a function of V_g and V at $T = 4.2$ K. The data are plotted as a gray scale. There is a gap around the origin where $dI/dV = 0$. This gap shows complex behavior as a function of V_g and is followed by a finite conductance region above $V \sim 25$ –50 mV. Qualitatively similar results have been obtained on a number of devices consisting of both ropes and single tubes (as determined by AFM measurements of the rope/tube height).

The data in Fig. 3 are highly reminiscent of measurements of the Coulomb blockade for a number of dots in series [19,20]. In these systems, an electron must hop through a series of quantum dots, each with a typical charging energy U , for current to flow. Since at any V_g , some of the dots will be blockaded, $dI/dV = 0$ at low energies. Thermal energies kT or finite bias energies eV

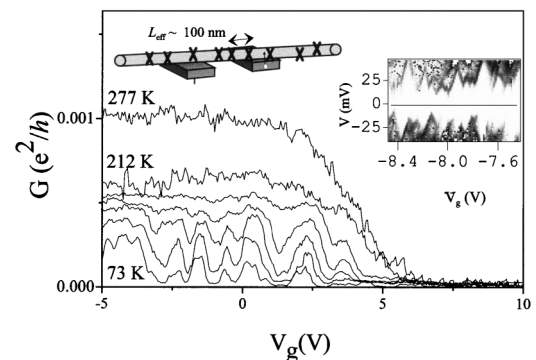


FIG. 3. G vs V_g for a semiconducting nanotube device with contacts separated by $0.5 \mu\text{m}$. The diameter of the tube (determined from its height in an AFM image) is 1.5 nm, consistent with a single SWNT. Holes are added to the tube below $V_g = 5$ V and the tube becomes conducting. Irregular Coulomb oscillations are observed below $T \sim 150$ K. The lower inset shows dI/dV vs V and V_g plotted as a gray scale for a second device at $T = 4.2$ K. Complex structure consistent with transport through a number of quantum dots in series is seen. The T dependence and typical charging energy indicates that the tube is broken up into segments of length $L_{\text{eff}} \sim 100$ nm, as indicated in the schematic.

on the order of U are required to overcome the Coulomb blockade and produce a finite conductance. We therefore conclude that in semiconducting tubes disorder effectively breaks the tube into a series of dots separated by tunnel barriers, as is schematically illustrated in the inset to Fig. 3. The conductance is thus determined by tunneling through a series of quantum dots.

We can estimate the size of these disorder-induced dots from the temperature and bias dependence of the Coulomb blockade features. Since the features appear at energy scales 100 times larger than for the metallic tube in Fig. 2, we find $L_{\text{eff}} \sim 100$ nm. Since the device is ~ 500 nm long, this implies that the effective sample consists of ~ 5 dots in series. From the conductance at room temperature, where charging effects are minimal, we estimate that the tunnel barriers between the dots each have transmission probabilities ~ 0.001 – 0.1 .

These measurements indicate that the diffusive transport model discussed previously—consisting of a large number of scatterers each with $T_i \sim \frac{1}{2}$ —is inappropriate for these samples. Instead, strong disorder over a much longer length scale better describes this system. It is still the case, however, that $G \ll e^2/h$, indicating that semiconducting tubes are much more strongly influenced by disorder than metallic tubes.

To understand this difference, we first review in detail the nature of the electronic states in graphite near E_f . The band structure in the vicinity of the \mathbf{K} (\mathbf{K}') point can be described within the $\mathbf{k} \cdot \mathbf{p}$ approximation by a 2D Dirac Hamiltonian for massless fermions, $H = \hbar v_F \boldsymbol{\sigma} \cdot \mathbf{k}$ [21]. Here \mathbf{k} is the wave vector measured relative to the \mathbf{K} (\mathbf{K}') point and the $\boldsymbol{\sigma}$'s are the Pauli matrices. This Hamiltonian is well known in both condensed-matter and particle physics; in the latter case, it is used to describe, e.g., a 2D massless neutrino. The states and their corresponding energies are given by [8,9,21]

$$|k\rangle = \frac{1}{\sqrt{2}} e^{i\mathbf{k}\cdot\mathbf{r}} \begin{pmatrix} -ibe^{-i\theta_k/2} \\ e^{i\theta_k/2} \end{pmatrix}; \quad E = b\hbar v_F |k|, \quad (1)$$

where θ_k is the angle that \mathbf{k} makes with the y axis in Fig. 1(a) and $b = 1(-1)$ for states above (below) the energy at \mathbf{K} . Equation (1) shows that, within this model, the electrons possess a two-component vector that gives the amplitude of the electronic wave function on the two sublattice atoms. This vector can be viewed as describing a “pseudospin,” in analogy to the two-component spinor describing the electron’s real (physical) spin. The direction of this pseudospin determines the character of the underlying molecular orbital state (e.g., bonding or antibonding—see Fig. 1). Inspection of Eq. (1) reveals that the pseudospin is tied to the \mathbf{k} vector such that it always points along \mathbf{k} . This is completely analogous to the physical spin of a massless neutrino which points along the direction of propagation. The states around \mathbf{K} correspond to right-handed neutrinos (pseudospin parallel to \mathbf{k}), whereas those around \mathbf{K}' are left-handed (pseudospin antiparallel

to \mathbf{k}). For the antiparticles ($b = -1$) this situation is reversed. Physically, this pseudospin means that the character of the underlying molecular orbital state depends upon the propagation direction. For example, a negative energy state near \mathbf{K} with a positive k_x is built from antibonding molecular orbitals while the state with $-k_x$ is built from bonding orbitals. This is schematically indicated in Fig. 1(b).

Following Ando and collaborators [8,9], we now consider scattering between these allowed states in a carbon nanotube due to *long-range disorder*, i.e., disorder with Fourier components $V(\mathbf{q})$ such that $\mathbf{q} \ll \mathbf{K}$. In this case, the disorder does not couple to the pseudospin portion of the wave function since the disorder potential is approximately constant on the scale of the interatomic distance. The resulting matrix element between states is then [8]: $|\langle k'|V(r)|k\rangle|^2 = |V(k - k')|^2 \cos^2[(1/2)\theta_{k,k'}]$, where $\theta_{k,k'}$ is the angle between the initial and final states. The first term is just the Fourier component at the difference in the k values of the initial and final envelope wave functions. The cosine term is the overlap of the initial and final spinor states.

For a metallic tube [Fig. 1(b)], backscattering in the massless subband corresponds to scattering between $|k_x\rangle$ and $|-k_x\rangle$. Such scattering is forbidden, however, since the molecular orbitals of these two states are orthogonal, as was clearly emphasized by Ando *et al.* [8,9]. In semiconducting tubes, however, the situation is quite different [Fig. 1(c)]. The angle between the initial and final states is $< \pi$, and scattering is thus only partially suppressed by the spinor overlap. As a result, semiconducting tubes should be sensitive to long-range disorder, while metallic tubes should not. Note that *short-range* disorder, $\mathbf{q} \sim \mathbf{K}$, will couple the molecular orbitals together and lead to scattering in all of the subbands.

To support this picture, we have performed tight-binding calculations of the conductance G of metallic and semiconducting tubes in the presence of a scattering potential. We employ the Landauer formalism to calculate the conductance from the transmission coefficients T_i of each subband. A three-dimensional Gaussian potential of the form $V(r) = V_0 \exp(-r^2/2\sigma^2)$ centered on one of the atoms on the nanotube wall is included in the tight-binding Hamiltonian. The transmission coefficients are obtained from boundary condition matching between the disorder-free region and the disordered region.

In Fig. 4, the calculated $G(E)$ is shown for two realizations of a single Gaussian scatterer with the same integrated strength but different widths corresponding to long-range (dashed lines) and short-range disorder (dash-dotted lines). The massless 1D band of a metallic tube is unaffected by a long-range scatterer, but there is significant backscattering of the states in the semiconducting tube in the region near the threshold for transmission. There is also backscattering of the higher subband states of the metallic tube, as is expected from extending the

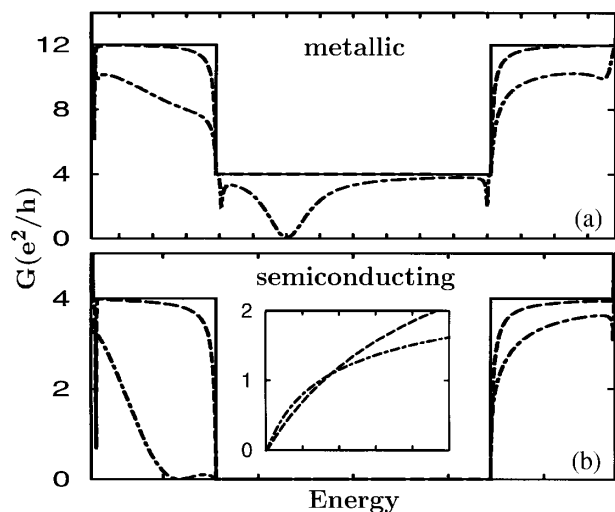


FIG. 4. Tight-binding calculation of the conductance of an (a) metallic (10,10) tube and (b) semiconducting (17,0) tube in the presence of a Gaussian scatterer. The energy scale on the abscissa is 0.2 eV per division in both graphs. The solid lines show the results for a disorder free tube, while the dash and the dot-dashed lines are for, respectively, a single long-range ($\sigma = 0.348$ nm, $\Delta V = 0.5$ eV) and short-range ($\sigma = 0.116$ nm, $\Delta V = 10$ eV) scatterer centered on the wall of the tube. Here ΔV is the shift in the on-site energy at the potential center. The massless band of the metallic tube is unaffected by the long-range scatterer, unlike the massive bands of the metallic and semiconducting tube. All subbands are influenced by the short-range scatterer. The inset shows an expanded view of the onset of conduction in the semiconducting tube at positive E , with each division corresponding to 1 meV. To compare to the experimental data, we estimate that a gate voltage change V_g of 1 V in Fig. 3 corresponds to a chemical potential change \bar{E} of the order of 1 meV.

arguments above. This calculation clearly demonstrates that the two types of subbands (massive and massless) are affected very differently by long-range disorder in a manner accurately captured by the physics of the pseudospin discussed above.

These theoretical considerations agree very well with the experimental results. Long range disorder due to, e.g., localized charges near the tube, breaks the semiconducting tube into a series of quantum dots with large barriers and a dramatically reduced conductance. Metallic tubes, on the other hand, are insensitive to this disorder and remain near-perfect 1D conductors. In the future, it will be of great interest to explore other experimental

manifestations of this pseudospin degree of freedom in graphene materials.

We wish acknowledge useful and enlightening discussions with Dung-Hai Lee and thank the Smalley group for the nanotube material used in these studies. Y. Yoon acknowledges discussions with Hyung Joon Choi and the use of his tight-binding code. This work was supported by DOE, Basic Energy Sciences, Materials Sciences Division, the sp^2 Materials Initiative, and by NSF DMR-9520554.

*Present address: Oersted Laboratory, Neils Bohr Institute, Universitetsparken 5, DK-2100 Copenhagen, Denmark.

- [1] M.S. Dresselhaus, G. Dresselhaus, and P.C. Eklund, *Science of Fullerenes and Carbon Nanotubes* (Academic, San Diego, 1996).
- [2] C. Dekker, *Phys. Today* **52**, No. 5, 22 (1999).
- [3] C. Kane, L. Balents, and M.P.A. Fisher, *Phys. Rev. Lett.* **79**, 5086 (1997).
- [4] Y. A. Krotov, D.-H. Lee, and S.G. Louie, *Phys. Rev. Lett.* **78**, 4245 (1997).
- [5] R. Egger and A.O. Gogolin, *Phys. Rev. Lett.* **79**, 5082 (1997).
- [6] M. Bockrath *et al.*, *Nature (London)* **397**, 598 (1999).
- [7] C.T. White and T.N. Todorov, *Nature (London)* **393**, 240 (1998).
- [8] T. Ando, T. Nakanishi, and R. Saito, *J. Phys. Soc. Jpn.* **67**, 2857 (1998).
- [9] T. Ando and T. Nakanishi, *J. Phys. Soc. Jpn.* **67**, 1704 (1998).
- [10] S.J. Tans *et al.*, *Nature (London)* **386**, 474 (1997).
- [11] M. Bockrath *et al.*, *Science* **275**, 1922 (1997).
- [12] S. Frank *et al.*, *Science* **280**, 1744 (1998).
- [13] A. Y. Kasumov *et al.*, *Science* **284**, 1508 (1999).
- [14] H. T. Soh *et al.*, *Appl. Phys. Lett.* **75**, 627 (1999).
- [15] S.J. Tans, R.M. Verschueren, and C. Dekker, *Nature (London)* **393**, 49 (1998).
- [16] R. Martel *et al.*, *Appl. Phys. Lett.* **73**, 2447 (1998).
- [17] A. Bezryadin *et al.*, *Phys. Rev. Lett.* **80**, 4036 (1998).
- [18] M. Bockrath *et al.*, report, 1999.
- [19] A. A. M. Staring, H. van Houten, and C.W.J. Beenakker, *Phys. Rev. B* **45**, 9222 (1992).
- [20] V. Chandrasekhar, Z. Ovadyahu, and R.A. Webb, *Phys. Rev. Lett.* **67**, 2862 (1991).
- [21] C.L. Kane and E.J. Mele, *Phys. Rev. Lett.* **78**, 1932 (1997).